

Tidal debris of dwarf spheroidals as a probe of structure formation models

Lucio Mayer¹, Ben Moore², Thomas Quinn¹, Fabio Governato³, Joachim Stadel⁴

¹ Department of Astronomy, University of Washington, Seattle, WA 98195, USA mayer@astro.washington.edu, trq@astro.washington.edu

² Department of Physics, University of Durham, South Road, DH1 3LE, Durham, UK, Ben.Moore@durham.ac.uk

³ Osservatorio Astronomico di Brera, via Bianchi 46, I-23807 Merate (LC) – Italy, fabio@merate.mi.astro.it

⁴ University of Victoria, Department of Physics and Astronomy, 3800 Finnerty Road, Elliot Building, Victoria, BC V8W 3P8 Canada, stadel@phys.uvic.ca

10 April 2024

ABSTRACT

Recent observations suggest that Carina and other nearby dwarf spheroidal galaxies (dSphs) are surrounded by unbound stars tidally stripped by the Milky Way. We run high-resolution N-Body simulations of dwarf galaxies orbiting within the Milky Way halo to determine if such observations can be explained with dark matter potentials as those implied by current structure formation models. We show that tidal forces acting on dwarfs with constant density cores or with cuspy profiles having a low concentration parameter ($c < 5$) lead to flat outer stellar density profiles like that of Carina for a variety of orbital configurations. On the contrary, it is more difficult to remove stars from cuspy dark matter halos with concentrations as high as predicted by CDM models at the mass scale of dwarf galaxies ($c > 10$) and the data can only be reproduced assuming nearly radial orbits. Our simulations show that Carina is losing mass at a fractional rate $< 0.1 \text{ Gyr}^{-1}$ and its mass-to-light ratio could be inflated by at most a factor of 2 due to unbound stars projected along the line of sight. We follow the evolution of the tidal debris within a triaxial clumpy cold dark matter Milky Way halo which causes differential precession and small-scale heating of the stellar streams. This renders their use as a dynamical tracer of the Galactic potential practically useless, but does provide a novel test of the nature of the dark matter. Models with warm dark matter (WDM) or collisional fluid dark matter (FDM) produce dwarf halos with lower central densities than CDM and would be consistent with the observed tidal tails even for orbits with eccentricities as low as indicated by current data on nearby dwarf spheroidals. Galactic halos in FDM are smooth and spherical and would be favored by the detection of cold coherent streams such as that associated with the Sagittarius dwarf spheroidal.

Key words: galaxies: Local Group | galaxies: dwarfs | galaxies: evolution | galaxies: interactions | cosmology: dark matter | methods: N-Body simulations

1 INTRODUCTION

In hierarchical models of structure formation the first dark matter clumps that eventually host luminous galaxies have masses comparable to the smallest dwarf galaxies in the Local Group (Haiman, Thoul & Loeb 1996, Haiman, Rees & Loeb 1996, Tegmark et al. 1997). In these models dwarf galaxies represent the cornerstones of galaxy formation; observations of dwarf galaxies should thus provide fundamental tests to our current understanding of how structure formation has proceeded in the Universe. Some of the properties of dwarf galaxy populations in the Local Group and other nearby groups (Grebbe et al. 2001) can be understood within

the hierarchical clustering scenario; the morphology-density relation, namely the fact that dwarf spheroidals (dSphs) are clustered around the dominant galaxies in the groups while dIrrs are found at much larger distances from them (Mateo 1998; Grebel 2000) likely reflects the continuous transformation of dIrrs into dSphs as they fall into the overdensity of the group and are stirred by the tidal field of the primary galaxies (Mayer et al. 2001a,b). On the other hand, the currently popular incarnations of hierarchical scenarios, namely cold dark matter models, are challenged by the apparent dearth of small satellites below $V_c = 30 \text{ km/s}$ (Moore et al. 1999; Klypin et al. 1999) and by the rotation curves of

dIrrs and LSB galaxies, that suggest that their halos have constant density cores instead of the predicted steep cusps (Cote et al. 1997; Lake & Skillman 1991; de Blok & McGaugh 1997; de Blok et al. 2001; McGaugh, Rubin & de Blok 2001; Van den Bosch et al. 2001). These problems have recently motivated the exploration of alternative models, such as self-interacting dark matter (SIDM, Spergel & Steinhardt 2000, Moore et al. 2000, Yoshida et al. 2000a,b; Fimiani et al. 2000a,b; Hogan et al.), warm-dark matter (WDM) (Bode et al. 2001; Dalcanton & Hogan 2001; Avila-Reese et al. 2001) and fluid dark matter (FDM) (Peebles & Villenkin 1999; Peebles 2000).

Dwarf spheroidal galaxies in the Local Group are the faintest galaxies known in the Universe to date ($M_B > 12$) and, in the traditional view, their large velocity dispersions reflect high dark matter contents (Mateo 1998). The long-lasting tidal interaction with the Milky Way and M31 should strip stars and dark matter from their potentials, leading to the formation of stellar and dark matter streams orbiting within the halo of the primaries (Johnston et al. 1998; Ibata et al. 1998; Helmi & White 1999). Observational evidence of streams associated with tidally stripped dwarfs, such as Sagittarius, is constantly accumulating in the stellar halo of the Milky Way (Helmi et al. 2000, 2001; Martinez-Delgado et al. 2000, Ibata et al. 2001; Dohm-Palmer et al. 2001; Vivas et al. 2001) and, more recently, even around the nearby Andromeda galaxy (Ibata et al. 2001b). For more distant dSphs the attenuating of the star counts in the vicinity of the nominal tidal radius (Irw in & Hatzidimitriou 1995) has been often interpreted as a signature of the presence of tidal tails (Johnston et al. 1999). However, some authors have argued that such peculiar profiles indicate that the dwarfs are not bound and thus no dark matter would be needed to explain the large velocity dispersions (Kuhn & Miller 1989; Klessen & Kroupa 1995). Recently, observations that take advantage of wide field photometry have confirmed the attenuating of the star counts out to larger radii in Carina (Majewski et al. 2000; Kuhn et al. 1999), while the cases of Draco (Piatek et al. 2001) and Ursa Minor (Martinez-Delgado et al. 2001) are still controversial. Majewski et al. claim on the basis of the observed extra-tidal extension, that Carina must have experienced a very large mass loss rate, losing more than 90% of its initial mass in 10 Gyr due to stripping by the Milky Way's tides.

The size and mass of unbound structures originating from the galaxies must be determined by both the typical densities of the latter (including dark matter) and the scale-length of their stellar components. Very dense systems, or systems with stellar components whose size is such that they lie well inside the tidal radius, will be harder to strip (Moore 1996). In CDM models dark matter halos have cuspy profiles with inner slopes $\propto r^{-1}$ or steeper (Dubinski & Carlberg 1991, Navarro et al. 1997; Moore et al. 1999b; Ghigna et al. 2000), but their typical densities within the radius of the stellar component, measured by the concentration $c = r_t/r_s$ (where r_s is the characteristic scale radius and r_t is the tidal radius) can vary considerably (Bullock et al. 2000); the higher is the concentration the steeper is the rise of the rotation curve and hence the local escape speed will be also higher.

It has been shown that there is enough freedom in the structural parameters allowed by CDM for large galaxies in

the process of merging to form massive tails as observed (Dubinski et al. 1996; Mihos et al. 1998; Springel & White 1999). However, these conclusions cannot be trivially extended to smaller mass scales because the typical concentration of halos (and thus their central density) increases substantially with decreasing mass in CDM cosmologies. Moreover, the choice of the orbital parameters of the interacting systems also plays a role by defining both the typical intensity and the time dependence of the external tidal forces; for the dwarf satellites of the Milky Way and M31, we have distances and some information on the orbits themselves (Mateo 1998), which allows us to constrain the parameter space better than in the case of more remote binary systems. In addition, the subsequent evolution of the material stripped from dwarf satellites can provide useful information on the potential of the Milky Way and M31; in fact, the orbits that the tidal debris will follow will reflect the underlying mass distribution.

In order to explore the role of tidal effects on stellar systems embedded in halos analogous to those forming in cold dark matter models, we have carried out several high-resolution N-body simulations of dwarf galaxies interacting with the external potential of the Milky Way. The simulations were performed with PKDGRAV, a fast, parallel binary tree code (Dikaiakos & Stadel 1996; Stadel, Quinn & Wadsley 2002). The paper is organized as follows: in the next section we will provide a description of the models used for the dwarf galaxies, section 3 will be devoted to the results of the simulation, and finally we will discuss and summarize our findings.

2. INITIAL CONDITIONS

Many previous studies that investigated the tidal disruption of dSphs (Johnston et al. 1997; Ibata et al. 1998; Klessen & Kroupa 1998; Helmi & White 1999) employed spherical King models to represent their mass distribution and placed them on mostly circular orbits in the potential of the primary halo. The structure and orbits of the galaxies were thus detached from the predictions of structure formation models. We use more sophisticated models of dwarf satellites, whose halo masses, sizes and density profiles are consistent with those of objects already in place at $z = 1$ in hierarchical cosmologies (White & Frenk 1991), the dSphs being at least as old. The initial dwarf models are placed on bound orbits in the Milky Way halo, which is modeled by the external potential of an isothermal sphere with mass $M_{\text{prim}} = 3 \cdot 10^{12} M_\odot$, circular velocity $V_{\text{prim}} = 220$ km/s, virial radius $R_{\text{prim}} = 400$ kpc and core radius of 4 kpc (see Mayer et al. 2001b for more details). The dwarfs are rotationally supported, exponential disks embedded in truncated isothermal halos with a core or within NFW halos (Hemquist 1993; Springel & White 1999) and resemble observed dIrrs. Disks and halos are sampled by $5 \cdot 10^4$ and $3.5 \cdot 10^5$ particles, respectively. After several orbits the dwarfs will be transformed into dSphs and will satisfy the morphology-density relation (Mayer et al. 2001a,b).

The halos are exponentially truncated at $r_t = R_{200}$, where R_{200} is their virial radius (i.e. the radius enclosing an overdensity equivalent to 200 times the average density of the Universe). In particular, here we consider models

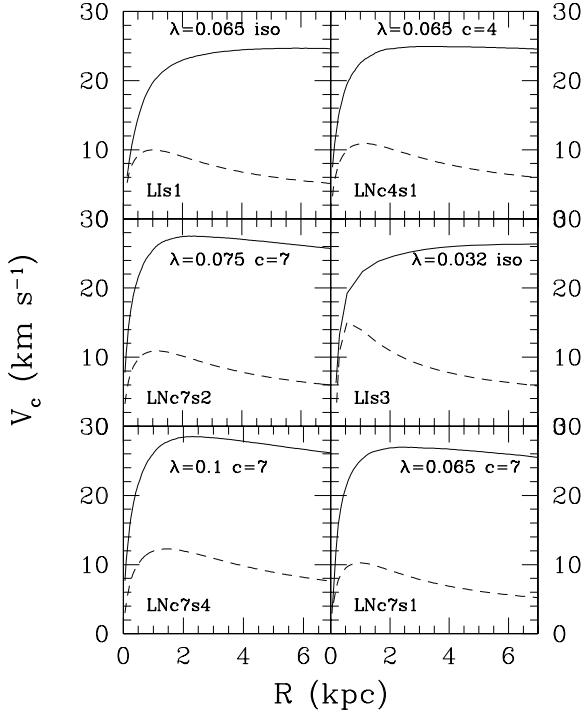


Figure 1. Rotation curves of initial model galaxies for the smallest mass scale considered ($V_c = 25$ km/s, $M_{\text{sat}} = 3 \times 10^4 M_{\text{prim}}$). The other mass models are simply rescaled versions of those shown here, as explained in the text. In the panels the spin and concentration c (the latter only for the satellites with NFW halos) are indicated. We recall that the isothermal models have a fixed core radius $r_c = 0.035 r_t$, while the disk scale length varies according to λ . The related model names (used throughout the text) are in the left bottom corner of each panel.

of low-surface brightness (LSB) dIrrs because these are the likely progenitors of dSphs (Mayer et al. 2001a,b). The models with truncated isothermal halos have a constant density core with radius r_c such that $r_c = 0.035 r_t$. Models with NFW halos are characterized by the concentration $c = r_t/r_s$, where r_s is the characteristic scale length of the halo, namely the radius at which the slope of the profile changes from r^{-3} to r^{-1} (Navarro et al. 1996, 1997); we consider models with either $c = 4$ or $c = 7$. The satellites span a range in initial circular velocities, from $V_c = 20$ km/s to $V_c = 75$ km/s; across such a mass range the typical concentration of halos in LCDM models is $c \approx 9$ (Eke et al. 2001). The surface density of the disks is kept fixed (except in model LIs3 and in the model described in section 4) and corresponds to a central (B band) surface brightness $\Sigma_B = 23.5$ mag arcsec $^{-2}$ assuming a stellar mass-to-light ratio (M/L_B) = 2 (Bottema 1996; de Blok & McGaugh 1997). Models of different masses are simply rescaled using the cosmological scaling between virial mass, virial radius and circular velocity (Mo et al. 1998). The details of the procedure used to assign the structural parameters of the halo and disks of the satellites are explained in Mayer et al. (2001) and Mayer et al. (2001b).

The models employed in this paper include a major improvement in that the scale length of the disks, r_h , instead

of being a free parameter, is determined by the structural parameters of the dark halo, as in current galaxy formation models. In the latter models it is assumed that the specific angular momentum of the gas, bound to the dark halo, that cools and eventually fall towards the center forming the stellar disk is initially equal to that of the halo and is conserved during the infall (Fall & Efstathiou 1980; Mo et al. 1998). In the simplest model in which the dark matter halo is a singular isothermal sphere, we have $r_h = 1/\sqrt{2} R_{200}$, where λ is the spin parameter, which measures the amount of kinetic energy stored into rotation, $\lambda = J/E^{1/2} = GM^{5/2}$ (E is the binding energy and J is the total angular momentum of the halo). N-body simulations show that the spin parameter of large samples of halos follows a log-normal distribution, with mean values in the range 0.035–0.05 and dispersions 0.6 (Barnes & Efstathiou 1987; Warren et al. 1992; Gardner 2001).

Our reference isothermal LSB models (LIs1, see Figure 1) have scale-lengths corresponding to $\lambda = 0.065$ (i.e. slightly above the average values); the resulting scale length is equal to the core radius of the halo, this being consistent with the analysis of rotation curves in the sample of dIrrs/LSB galaxies in de Blok & McGaugh (1997). We also consider a model with the same r_c but r_h lowered by a factor of 2 which corresponds to a smaller spin parameter, $\lambda = 0.035$ (model LIs3, in Figure 1); this model has the same disk mass of model LIs1, and thus the central surface brightness is $\Sigma_B = 22$ mag arcsec $^{-2}$ (1.5 magnitudes higher than the standard value).

In more realistic NFW halos the scale length of the disks depends not only on λ but also on the concentration c and on the halo/disk mass ratio; the more baryons accumulate in the center, the more the whole system contracts in response and thus the smaller is the initial scale-length of the baryons. All these aspects are taken into account in the algorithm used for building the galaxies (see Springel & White 1999) but, for the sake of simplicity, we keep the halo/disk mass ratio close to 50 in all our models. The reference NFW model with $c = 7$ and $\lambda = 0.065$ (model LNc7s1 in Figure 1) has the same disk mass and radius of the isothermal model LIs1 but the rotation curve rises more steeply; the rotation curve of the isothermal model is better reproduced by a model with $c = 4$ (model LNc4s1 in Figure 1). We investigate also the effect of varying only λ at fixed c ; models LNc7s2 and LNc7s4 have $c = 7$ but $\lambda = 0.075$ and $\lambda = 0.1$, respectively (a value of λ as high as 0.1 is found in $< 30\%$ of halos in cosmological simulations).

We consider different orbital eccentricities, ranging from apo/per = 2 to apo/per = 15 and different disk orientations, although we neglect cases in which the satellites are on retrograde orbits, as it is well known that this configuration strongly inhibits the formation of tidal tails, irrespective of the internal structure of galaxies (Toomre & Toomre 1972; Dubinski et al. 1996; Springel & White 1999; Mayer et al. 2001a,b). The orbits have apocenters between 150 and 250 kpc and pericenters between 20 and 80 kpc, thus encompassing the whole range of galactocentric distances of dSphs.

3 RESULTS

Here we present the results of the simulations in three separate subsections; in 3.1 we will show that we are able to reproduce the observed outer profile of Carina and that this happens when the halo of the dwarf has a sufficiently shallow mass distribution or when the orbit is nearly radial; in 3.2 we will analyze the discrepancy between the intrinsic mass loss rates measured in the simulations and those inferred from the observations; finally, in 3.3 we will evolve the tidal debris of spherical dwarf models within a CDM halo extracted from a cosmological simulation and will show how the streams undergo precession and heating by substructure, losing their coherence and becoming difficult to detect.

3.1 Tidal features and the internal structure of satellites

The satellites are severely stripped by the Milky Way tides but a bound stellar and dark component survives until the end of the simulations (< 10 Gyr); after a few orbits (the orbital times are of the order of 2–3 Gyr), the stellar disk is transformed into a moderately triaxial system supported by velocity dispersion that closely resembles a dSph (see also Mayer et al. 2001a,b). Figure 2 shows the projected star counts from four representative simulations. In all cases we find tidal streams of stars escaping from the satellites which show up as a flattening of the outer projected star counts. The surface brightness of the tails depends strongly on the orbit and the structure of the initial models; the “strength” of the streams can be quantified simply by the surface density of stars compared to the centrally measured value, $\rho_0 = \rho_s$. Satellites with cored isothermal halos or low concentration ($c = 4$) NFW halos can reproduce very closely the extended flattened star counts observed in Carina (Majewski et al. 2000), for which $\rho_0 = \rho_s \approx 10^{-2}$. Moreover, the observations are reproduced even for orbits with moderate eccentricities (apo/peri = 2–3) for these initial galaxy models.

Instead, the streams are too weak to match the observations if the concentration is as high as $c \approx 7$, unless the orbits are nearly radial (Figure 2). In fact, raising the concentration by a factor of 2 leads to an increase of nearly 30% in the escape speed at the half mass radius of the stars where the rotation curve peaks. (This also increases their robustness to tides since its response will be more adiabatic, see section 3.2.) In this case $\rho_s = \rho_0 < 10^{-3}$. This is true even when the satellite is constructed with a considerably larger than the mean and thus acquires a larger disk scale-length (as in the case of the model LNC7s4 shown in Figure 2). In fact, the value of the concentration is the most important parameter in determining the amount of stripped material; a change in the spin affects only the disk-scale length, while a change in the concentration affects both the scale-length and the central density of the halo, or, equivalently, its local escape speed. However, if the initial disk scale-length is substantially decreased while keeping the disk mass fixed, the resulting higher surface density of the disk can affect its evolution enhancing the non-axisymmetric instabilities that drive the morphological transformation; in fact, in model LIS3, the high self-gravity of the compact disk leads to a strong bar instability and later to a very compact stellar

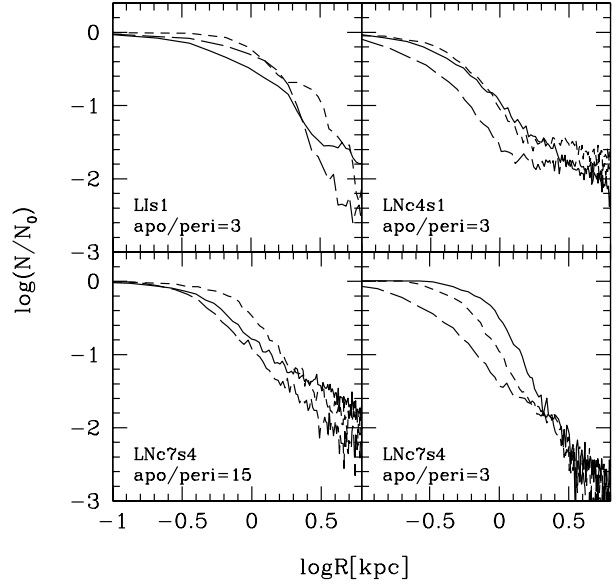


Figure 2. Projected star counts (after 7 Gyr) for representative remnants whose halos have all the same circular velocity, $V_c = 25$ km/s, corresponding to an initial total mass $M_{\text{sat}} = 10^{-4} M_{\text{prim}}$, where M_{prim} is the mass of the primary halo. In each panel we show the projected star counts obtained observing the stars along one of the tails (solid line) and along the two lines of sight perpendicular to the former (short dashed and long dashed lines). The names of the models employed and the orbital eccentricities are also indicated in the panels (the apocenter of the orbits is fixed at $R_{\text{apo}} = 270$ kpc, so the pericenter is as small as 18 kpc in the case of the most eccentric orbit). (see Figure 1 for the corresponding structural parameters).

remnant, thereby inhibiting the developing of tidal tails (see also Mayer et al. 2001b).

The simulations show that the visible strength of tidal extensions is sensitive to projection effects. The results by Majewski et al. (2000) show a strong flattening of the star counts at a distance comparable to the tidal radius of the dwarf galaxy, where the counts level out at 10^{-2} the peak value. The feature is more prominent when the line of sight of the observer falls along one of the tidal tails, because the projected surface density of the tails is maximally enhanced in this case. When viewed perpendicular to the orbit, the tails can be more easily separated from the bound stars visually, but in this case they have the lowest surface density (indeed corresponding to the actual intrinsic value), $\rho_B > 30$ mag arcsec $^{-2}$.

In Figure 3 we show in more detail the results for the satellite models LIS1 and LNC4s1 with $V_c = 25$ km/s (these have an initial total mass of only $5.8 \cdot 10^8 M_\odot$) as these yield remnants with physical scales close to those of Carina. In fact, we note that the flattening of the star counts occurs at 1–2 kpc from the center, the core radius of the bound remnant estimated from the fit with a King model with $c = 0.5$ is around 500 pc and the luminosity of the remnants is $M_B = 11$, assuming a gal stellar mass-to-light ratio of 5 (as derived by combining population synthesis models

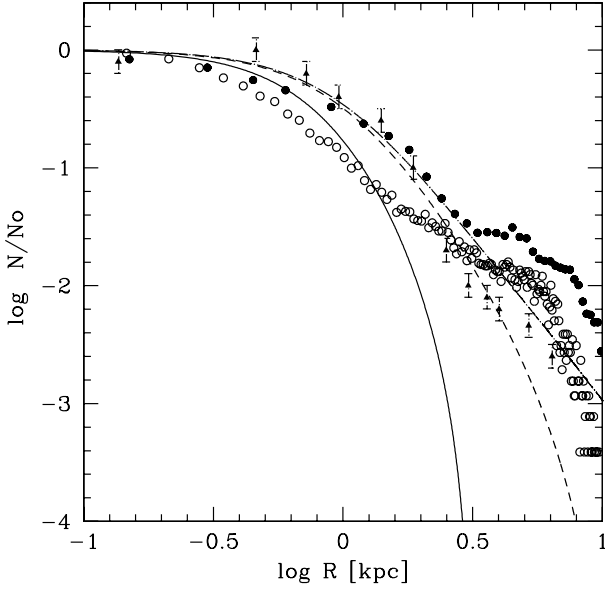


Figure 3. Projected star counts obtained for the remnant of model LIs1 (filled circles) and model LNc4s1 (open circles with $V_c = 25$ km/s, both observed along one of the tidal tails. The dots with error bars are the number counts from Majewski et al. (2000) averaged over the four samples of giant stars. Fits with King profiles with $c = 0.5, 1, 1.5$ (where $c = \log_{10}(r_t/r_c)$) are also shown (solid, short dashed and long dashed lines, respectively).

with a model for the star formation history as described in Mayer et al. (2001)). The total dark matter mass is almost 5 times higher than the stellar mass, yielding a central velocity dispersion ~ 10 km/s, as seen in Figure 4; the corresponding total $M=L$ would be around 25 for a stellar mass-to-light ratio of 5, in fairly good agreement with the observations (Mateo 1998) and comfortably higher than the lower limit obtained by Lake (1990) for galactic dwarf spheroidals.

In general, the presence of tidal extensions will lead to an overestimate in the velocity dispersions of the dwarf caused by unbound stars in projection; as already noted by others before (e.g. Piatek & Pryor 1992), a velocity gradient or an apparent rotation would also be observed due to the asymmetrical contamination introduced by tidal tails. However, in our simulations the apparent velocity dispersions in the central region of dwarfs are at most 40% larger than the intrinsic value, which would inflate the measured $M=L$ by no more than a factor 2 (giving $M=L < 50$ in the remnants LNc4s1 and LIs1). Figure 4 clearly shows that only measurements extending a few kpc from the center would be significantly altered; therefore the contamination of kinematics induced by tails would not explain the high mass-to-light ratios of dSphs without dark matter, contrary to previous claims (e.g. Kuhn & Miller 1989; Kuhn 1991).

Johnston et al. (1999) found that the contamination of streams in the projected star counts can show up even inside the intrinsic tidal radius of the satellites if the viewing angle is not perpendicular to the tails. We determined the tidal radii of our remnants with SKID, that identifies all the particles bound to the dwarf; we found that marginally

bound particles are found as far as 3-4 kpc from the center, namely at a larger distance than the break radius in any of the projections. However, this marginally bound region (that corresponds to the very inner part of the tails) comprises only a few percent of the total mass of the remnant. We conclude that, although the break radius is not equivalent to the tidal radius, it roughly defines the boundary of the remnant, encompassing $> 90\%$ of the bound mass.

3.2 Determining mass loss rates using extra-tidal stars

Estimating the mass loss rate of satellites from extra-tidal features is not a straightforward task. Johnston et al. (1999) have proposed a formula for estimating the mass loss rate of an orbiting stellar system which relies on the assumption that the number counts surface density profile of the extra-tidal material is $\propto r^{-1}$. Majewski et al. (2000) have applied such a formula to the star counts profile they obtain for Carina and derive an extremely large fractional mass loss rate, $df/dt = 0.3 \text{ Gyr}^{-1}$. This would imply that the mass of the stellar component in Carina would have been reduced by as much as a factor of 30 in 10 Gyr. We obtain comparable fractional mass loss rates applying the same formula to the remnants in our simulations, while the actual average fractional mass loss rates measured in the simulations (obtained by simply dividing the total mass lost by the duration of the simulation of about 10 Gyr) are significantly lower, $\sim 0.06 \text{ Gyr}^{-1}$.

One problem in the application of the formula is the assumed radial surface density profile of the stream. In fact, the outer star counts profile of our remnants are much flatter than r^{-1} for most of the viewing projections. Removing the constraint on the profile of the extra-tidal stars, Johnston et al. (1999) derive also an upper limit for the mass loss rate:

$$\frac{df}{dt} = \cos(\theta) \frac{n_{\text{xt}}(r_{\text{break}})}{n_{\text{break}}} \frac{2}{T_{\text{orb}}} r_{\text{break}}^2 \quad (1)$$

where θ is the angle between the velocity vector of the satellite and the line-of-sight (which can be derived for those satellites that have measured proper motions), n_{break} is the number of stars counted within r_{break} (the radius where the profile changes slope) and T_{orb} is the orbital time. Using equation (1) for the cases with clear tidal features we obtain $df/dt < 0.5 \text{ Gyr}^{-1}$, which is still not representative of the numerical results, being higher than the real mass loss rate by nearly an order of magnitude.

Equation (1) is derived under the assumption that the stars are lost continuously over the orbital time T_{orb} . However, the tidal mass loss for a satellite moving on an eccentric orbit will occur mostly as a result of the tidal shocks suffered at pericenter and will depend on its ability to respond to the perturbation and adjust to a new equilibrium. To gain a better insight into the mechanism, we can consider a galaxy that suffers a tidal shock of duration $\tau = R_p/V_p$, where R_p and V_p are, respectively, the distance and the velocity of the galaxy at the pericenter of the orbit. The characteristic time required for a star at the disk half mass radius r_{hm} to increase its mean-square velocity $\langle v^2 \rangle$ due to the shock is $t_{\text{shock}} = V_c^2 / \langle v^2 \rangle$, where V_c is the internal (rotational) velocity of the galaxy and v is the velocity

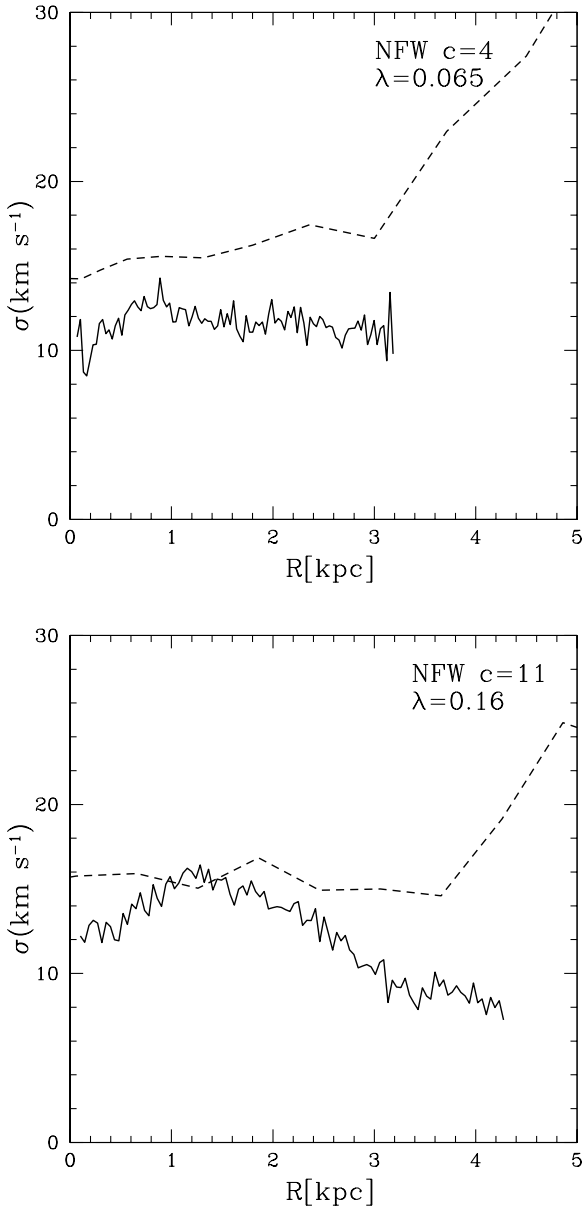


Figure 4. Intrinsic (solid line) versus apparent stellar velocity dispersion profiles (dashed line) for a line of sight that intercepts one of the tidal tails. The models used in the simulations are LNc4sl (upper panel) and the model with a highly concentrated halo and a large disk discussed in section 4.1. The orbits have apo/per= 2, with $R_p = 55$ kpc and both have halos with an initial circular velocity $V_c = 25$ km s⁻¹.

impulse; this time scale will be comparable to the characteristic time scale of mass loss (see Binney & Tremaine, 1987). Gnedin, Hemquist & Ostriker (1999) have provided analytical formulas to calculate $\langle v^2 \rangle$ for a satellite that is shocked by an extended perturber with an isothermal profile including even the adiabatic corrections that account for the motion of the stars within the galaxy. As shown by the authors, if the orbits are eccentric, a good approximation is obtained by simply assuming that the satellite is moving on a straight path. In the latter case we can write

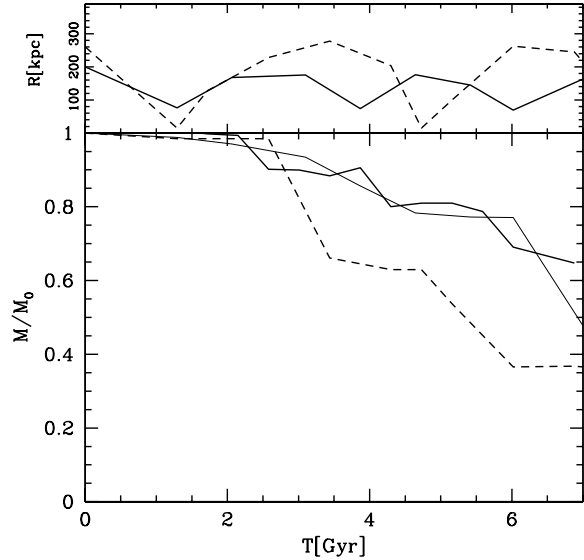


Figure 5. Fractional mass loss over 7 Gyr for satellites on a orbit with apo/per= 3 and $R_p = 75$ kpc (the thick solid line refers to model LNc4sl and the thin solid line to model LNc4sl) and on a orbit with apo/per= 15 and $R_p = 20$ kpc (the dashed line, corresponding to model LNc4sl).

$$\langle v^2 \rangle = \frac{GM_0}{R_p^2 V_p} \frac{r^2}{3} \frac{R_p^2}{R_{max}^2} (1 + \dots)^{2.5} \quad (2)$$

where M_0 and R_{max} are the total mass and radius of the perturber and the last term in the product is the first-order adiabatic correction (ω is the typical stellar frequency at $r = r_{hm}$, and $\omega = \omega_{dyn} / 1$ in our models, where ω_{dyn} is the dynamical time at $r = r_{hm}$). For a satellite with $V_c = 25$ km/s and $r_{hm} = 2$ kpc on the apo/per= 3 orbits in our simulations ($R_p = 75$ kpc, $V_p = 300$ km/s), we obtain $t_{shock} \approx 5$ Gyr. We can consider t_{shock} as an estimate of the characteristic time over which the satellite loses 50% of its initial disk mass.

As we can see from Figure 5, the satellites on apo/per= 3 orbits actually have lost about 40% of their mass 5 Gyr after the first tidal shock. Although in the simulations more than one shock occurs, the non-axisymmetric instabilities have a counteracting effect, as they make the stellar component more concentrated and increase the adiabatic corrections over time (see Mayer et al. 2001b), thereby explaining the good agreement with the above simple estimate.

The resulting average fractional mass loss rate is 0.1 ± 0.05 Gyr⁻¹. The agreement with the simulations strongly depends on the adiabatic corrections; if we neglect them then the resulting mass loss rate would be higher by a factor of 5 and would be close to the predictions of Johnston et al. (1999). In the inner regions of the system the adiabatic corrections will be increasingly more important and will increase substantially the overall lifetime of the satellite.

Using the numerical results as a guide we propose a simple recipe to infer the mass loss rate from the observed star counts profile; on typical orbits as those considered here the dwarfs lose mass at a rate that scales as $\dot{M} \propto (r_s = 0)$;

employing the simulations that match the data on Carina to calibrate our estimate (these yield a fractional mass loss rate $df/dt = 0.06 \text{ Gyr}^{-1}$), we obtain $df/dt = 6\% \text{ (} s=0 \text{)}$ Gyr^{-1} . This result was derived for the satellites on orbits with apo/per = 3, but the mass loss rates on nearly radial orbits differ by less than a factor of 2 (see Figure 5).

3.3 Precession and heating of tidal streams

For dwarfs orbiting in spherical and smooth potentials like those considered so far the escaping stars form symmetric tidal tails that lead and trail the satellite revealing its future and past orbit (see also Moore & Davis 1994). However, in general the orbital evolution of the streams will depend on the structure of the underlying potential and in turn the stream might be used as a tracer of such structure only provided that they remain sufficiently coherent (Johnston et al. 1999a, Zhao et al. 1999). Cold dark matter halos are complex triaxial systems with shapes and angular momenta that vary considerably from the center to their virial radii (Moore et al. 2001). They also contain dark matter substructure and satellite galaxies that can heat and perturb parts of the stream away from their orbital paths. These effects might combine to destroy the coherent nature of tidal streams through differential precession of orbits (see also Johnston, Sackett & Bullock 2001).

To investigate the long-term evolution of tidal tails we construct a massless spherical system using 50,000 particles distributed with a density profile $\rho(r)/r^{-1}$, radius 10 kpc and velocity dispersion $\sigma_{1d} = 10 \text{ km/s}$. This unbound test satellite will form tidal streams that can be used to explore orbits within different halos. The evolution of this system on a series of circular orbits within a smooth spherical potential is shown in Figure 6. This potential is a singular dark matter halo with density profile $\rho_p(r)/r^{-2}$ with constant velocity dispersion $\sigma_{\text{halo}} = 200\sqrt{2} \text{ km/s}$. The rings of debris correspond to satellites on initially circular orbits at radii of 0.2; 0.4; 0.6; 0.8; 1.0 r_{200} where $r_{200} = 300 \text{ kpc}$.

The satellite is unbound and immediately starts to form symmetric tidal tails because the model has a finite size and the particles have random velocities. The tidal debris lies in the orbital plane and after a time scale of 6 Gyrs the particles lie in streams that wrap around more than one orbit at the center of the potential and about 10% of an orbital radius at the edge.

We now repeat the test using a CDM halo taken from one of the cosmological simulations of Moore et al. (1999a). By construction, the circular velocity and virial radius are similar to those adopted in the spherical potential above. The halo is resolved with 10^6 particles within R_{200} and we use a comoving softening length of 0.5 kpc. This particular galactic mass halo virialises by a redshift $z = 0.5$ and does not accrete any bound object containing more than 1% of its mass by the present day. We calculate the axis with the largest component of angular momentum and place the test satellites in circular orbits at the same radii as used in the spherical potential above.

Figure 7 shows the satellite particles after a period of 6 Gyrs revealing that the tidal streams have precessed dramatically away from their initial orbits. The inner streams have wrapped several times around the halo, both within

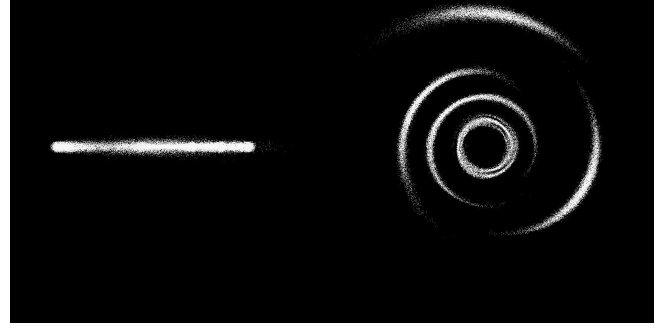


Figure 6. The evolution of five massless satellites on circular orbits within a smooth spherical potential for a period of 6 Gyr (comparable to the orbital time of the outer satellite). The left panel is an edge on view of the orbital plane and the right panel is a face on view.

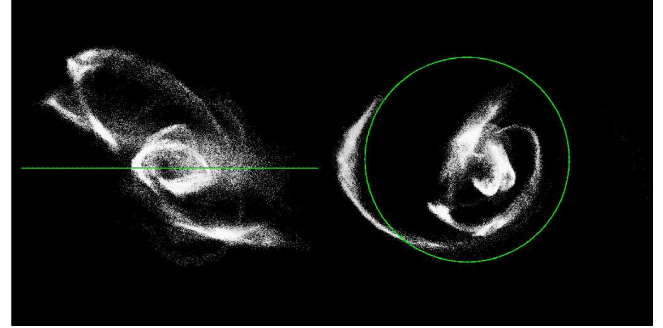


Figure 7. The evolution of 5 massless satellites on initially circular orbits (same as in Figure 6) within a CDM galactic mass halo. The satellites are introduced at a redshift $z = 0.5$ and the simulation is continued to the present day. The left panel is an edge on view of the initial orbital plane and the right panel is a face on view.

and out of the orbital plane whilst the outer streams remain more coherent but have precessed from their initial orbital plane by over 45 degrees. The precession from the differentially rotating triaxial halo structure is mostly responsible for the differences between the orbits of the tidal debris between Figure 6 and Figure 7. However, the substructure in the galactic CDM halo has also contributed visible heating to the streams. This is most noticeable in the outer streams which have a clumpy appearance due to heating by the most massive subhalos. (Dark matter substructure in the outer halo will be more massive and cause the most heating.) Numerical heating of the streams due to massive halo particles (Moore et al. 1996) might somewhat enhance the observed evolution of the streams. In order to test our results we ran a massless spherical satellite in a 10^5 particles Milky Way-sized halo with an NFW profile; this halo is similar to the CDM halo as far as profile, mass and radius are concerned but it is spherical and does not have substructure, therefore no physical heating or precession is expected. After 10 Gyr we measured fluctuations of only a few percent in the orbital energy and orbital angular momentum, and, correspondingly, the initial orbital plane of the satellite is barely altered; this shows that two-body heating has a negligible contribution to the evolution of the streams (this is a conser-

vative test since the CDM halo in the cosmological volume had a resolution almost ten times higher).

The experiment illustrated in this section ignores the dissipative effects of a baryonic component that would help regularise the structure of the inner dark matter halo. However, the outer halo would remain unaffected by the adiabatic contraction and this tends to produce oblate inner halos (Dubinski & Carlberg 1991). Coherent streams should only be found in the plane of the disk or on polar orbits. Our results suggest that using streams to constrain the potential structure of galactic halos will be complicated by these effects. Evidence of streams on great circles in galaxy and cluster halos would support models in which the dark matter behaves like a fluid. In this case, halos are highly spherical and contain less mass attached to subhalos due to ram-pressure stripping. Interestingly, the stream associated with the Sagittarius dwarf spheroidal appears as a great circle; Ibata et. (2001), based on the analysis of the latter, have recently argued that the Galactic halo must be nearly spherical between 16 and 60 kpc from the center.

4 DISCUSSION

We have shown that the outer flattening observed in the stellar profiles of some dSphs can provide a useful constraint on the structure of their dark matter halos once their orbital eccentricity is known. At present, the few proper motions available (e.g. Kroupa & Bastian 1997 for the LMC and SMC, Schweitzer et al. 1995 for Sculptor and Schweitzer & Cudworth 1996 for Ursa Minor) imply that the Galactic satellites have orbits with low eccentricities, with typical apo/peri = 2–3. It is clear that systems on these orbits with concentrations as high as predicted in the standard LCDM cosmology (Eke et al. 2000) for galaxies with $V_c < 50$ km/s ($c \approx 9$) would not be able to reproduce the observed star counts of the Carina dSph.

One might argue that the properties of halos in CDM models have a large scatter. However, recently Bullock et al. (2001) have measured the scatter of the concentration of halo profiles in LCDM simulations and, according to their results, a concentration of $c = 7$ is already a lower limit for halos with $M = 10^{11} M_\odot$ (i.e. corresponding to the most massive among the models considered in this paper), suggesting that we are being conservative with our constraints.

Satellites with either softened isothermal halos or cuspy halos with low concentrations, exhibit features that can reproduce the observations (even on orbits with moderate eccentricities). Interestingly we note that the values of the concentration needed ($c < 5$) are as low as those found within WDM models at the dwarf galaxy scale (Eke et al. 2001).

4.1 High mass to light ratios in dSphs

Our results have implications on the actual dark matter content of dSphs. Large tidal tails are produced only when the dark matter in the remnants accounts for $\approx 80\%$ of the total mass. The apparent M/L can be at most two times higher than the intrinsic value because of the unbound stars projected along the line of sight and therefore we expect to find tidal tails only around dwarfs whose measured M/L is

not very high. Indeed most of the dSphs in the Local Group, including Carina, have $M/L \approx 30$ (Mateo 1998).

The dark matter contents of Draco and Ursa Minor, having $M/L > 60$ (Hargreaves et al. 1994a,b, Mateo 1998) are instead too high even accounting for enhanced apparent velocity dispersions. Such high dark matter contents would be incompatible with the observations of massive tails; the remnants that have similarly large dark matter contents at the end of our simulations (see also Mayer et al. (2001a,b) on the evolution of the GR8 model) have star counts at the level $\Sigma_{\text{obs}} = 0 < 10^{-3}$ in the outer part.

Although very recent results exclude the presence of tails in Draco (Odenkirchen et al. 2001; Aparicio et al. 2001), other authors have reported positive detections of some extra tidal stars around the latter dwarf and Ursa Minor (Piatek et al. 2001, Martínez-Delgado et al. (2001)). In order to further explore this issue we ran a simulation with a satellite model different from those used so far. We used an NFW halo with a high concentration, $c = 11$, and $V_c = 25$ km/s, and a disk extending out to half of the virial radius of the halo, ≈ 10 kpc, corresponding to a high spin parameter, $\lambda = 0.16$, and a very low central surface brightness, $\Sigma_B \approx 25$ mag arcsec $^{-2}$.

We placed the model on an orbit with an apo/peri = 2 and a pericenter $R_p = 55$ kpc, consistent with the present distances and radial velocities of Draco and Ursa Minor (Mateo 1998). After 7 Gyr the satellite has turned into a dSph ($v_{\text{rot}} \approx 0.3$) with a central velocity dispersion ≈ 10 km/s and a dark matter halo still 7 times more massive than the stellar component; this would yield $M/L > 40$ for a stellar mass-to-light ratio ≈ 5 (Mayer et al. 2001b). Furthermore, due to its unusually large scale length, the stellar component has undergone severe stripping, producing prominent tidal tails and signatures in the star count profile qualitatively similar to those observed in Carina (Figure 8); including possible projection effects due to the tidal tails, the apparent mass-to-light ratio could be enhanced up to values around 80. This experiment shows that an extremely extended disk can produce large tails notwithstanding the high central dark matter density of the halo. However, a closer look shows that the remnant is very extended in radius and the flattening of the star counts in the remnants occurs at more than 4 kpc, which is too far out compared to the size of Draco, the latter being less than 1 kpc (Mateo 1998). In addition, a dwarf progenitor with an extremely extended disk is hard to support from the observational point of view; the rotation curves of dIrrs and LSB spirals suggest that the scale-lengths of halos and baryons are correlated (de Blok & McGaugh 1997) and in some cases the scale-length of the halo can be larger than the typical disk size (Lake & Skillman 1990), while in the present model is considerably smaller. In the present model would clearly cause. Besides, the surface density of the gas in the outer part of such an extended disk would be so low that the star formation would have hardly occurred, making the formation of stellar tails unlikely.

The correct evaluation of the M/L of dSphs is important when one tries to compare the observed number of Galactic satellites with the numbers predicted by cosmological N-body simulations (Moore et al. 1999; Klypin et al. 1999). It has been pointed out that dwarfs with NFW halos should have rising velocity dispersion profiles and that

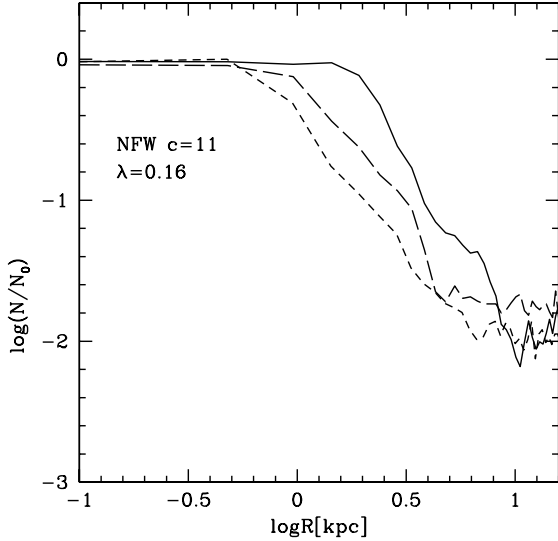


Figure 8. Projected star counts for the remnant (after 7 Gyr) of a satellite model with a highly concentrated halo. The satellite has $V_c = 25 \text{ km s}^{-1}$ and was placed on a orbit with apo/per = 2 and $R_p = 55 \text{ kpc}$. We show the projected star counts along one of the tails (solid line) and along the two lines of sight perpendicular to the former (short dashed and long dashed lines).

by using the measured central velocity dispersions one would actually underestimate the total mass of dSphs (White 2000); including this correction would improve the agreement with observations (Moore 2001).

Our simulations suggest two possible scenarios with regard to this issue and both are highlighted in Figure 4. First, if it were confirmed that most of the satellites have large tidal tails and that their orbits have low eccentricity, then it is very likely that their halos have low concentrations, $c < 7$, and have quite flat intrinsic and apparent velocity dispersion profiles; the apparent velocity dispersion can actually be higher than any value of the intrinsic velocity dispersion, but never smaller, which would actually tend to reverse the correction, (cfr. Figure 4a). Secondly, even if the satellites had more concentrated NFW halos (1) the intrinsic peak velocity dispersion is only 25% higher than the central value in the remnants and (2) the intervening tidal debris, though quite weak, tend to attenuate even further the apparent velocity dispersion profile (cfr. Figure 4b). Hence, it seems that a better assessment of the actual mass of the dwarfs derived from apparent velocity dispersions would never solve the substructure problem and could actually make it worse.

5 SUMMARY

We have used numerical simulations of two component models of dwarf galaxies orbiting within a Milky Way potential to study the effects related to their tidal tails. The signatures produced by the tidal debris in the stellar profiles can be used to constrain the structure of the dark matter halos of dwarfs, providing hints to the nature of the dark matter. The long term evolution of tidal debris was followed within

a smooth spherical potential and within a high resolution cold dark matter halo. We summarize our conclusions here:

We can produce tails as prominent as observed around the Carina dSph for models with soft central potentials or singular potentials on highly radial orbits. Knowledge of the orbits of the dSphs is vital to constrain directly their internal structure. If it will be confirmed that the orbits are nearly circular, warm dark matter models will be favored instead of cold dark matter.

Models with very high mass to light ratios and strong tidal tails are very difficult to produce. Draco and Ursa Minor should only have very weak tails, at a star count level at least ten times lower than that found in Carina.

Our simulations provide a simple estimate of the mass loss rates of dSphs based on star counts and these are significantly lower than those obtained by others discarding adiabatic corrections; Carina is likely to survive for at least another 5 Gyr.

Only satellites on very tightly bound orbits like Sagittarius, that suffered many strong tidal shocks, could have been already destroyed in the past or could be now close to disruption.

Central velocity dispersions of stars in dSphs are good indicators of the characteristic peak velocity dispersions of their dark matter halos. i.e. tidal heating produces nearly isotropic orbits and quite flat velocity dispersion profiles.

The masses of dwarf spheroidals could be overestimated when large tidal tails are present but the maximum effect due to projection of unbound stars is only a factor of two. However, this would shift the mass function of galactic satellites further away from that predicted by cold dark matter models, making the substructure problem even worse.

The tidal debris within a cold dark matter halo shows dramatic signatures of differential precession and some heating by dark matter substructures. It may be impossible to use observations of tidal streams to map the structure of the Galactic halo.

If many examples of coherent tidal streams are discovered, then this would favor fluid dark matter models which produce smoother and highly spherical dark matter halos.

6 ACKNOWLEDGEMENTS

The simulations were performed on the ORIGIN 3800 at the CINECA Supercomputing Center in Bologna and on an ALPHA workstation at the University of Washington. L.M. thanks Volker Springel for providing the code used to construct the galaxy models and Elena d'Onglia for providing the algorithm to track King profiles to the simulations. L.M. was supported by the National Science Foundation (NSF Grant 9973209).

REFERENCES

- Aparicio, A., Carrera, R., Martínez-Delgado, D. 2001, to appear on A J
- Avila-Reese, V., Colin, P., Valenzuela, O., D'Onglia, E., Firmani, C. 2001, to appear on ApJ
- Bames, J., Efsthathiou, G. 1987, ApJ, 319, 575
- Binney, J., & Tremaine, S. 1987, Galactic Dynamics (Princeton University Press)

- Bode, P., Ostriker, J., & Turok, N. 2001, *ApJ*, 556, 93
- Bottin, R. 1997, *A & A*, 328, 517
- Bullock, J. S., Kolatt, T. S., Sigad, Y., Somerville, R. S., Klypin, A. V., Klypin, A. A., Primack, J. R., & Dekel, A. 2001, *MNRAS*, 321, 559
- Cote, S., Freeman, K. C., & Carignan, C. 1997, *ASP conference series*, Vol. 117, 52
- Dalcanton, J. F. & Hogan, C. J. 2000, preprint (astro-ph/0004381)
- de Blok, W. J. G., & McGaugh, S. S. 1997, *MNRAS*, 290, 533
- de Blok, W. J. G.; McGaugh, S. S.; Bosma, A., Rubin, V. C. 2001, *ApJ*, 552, L23
- Dikaikos, M., & Stadel, J. 1996, *Conf. Proc. of the International Conference on Supercomputing* (New York: Assoc. for Computing Machinery)
- Dohm-Palmer, R. C., Helmi, A., Morrison, H., Mateo, M., Olszewski, E. W., Harding, P., Freeman, K. C., Norris, J., & Shectman, S. 2001, *ApJL*, L37, 555
- Dubinski, J., & Carlberg, R. 1991, *ApJ*, 478, 496
- Dubinski, J., Mihos, C., & Hernquist, L. 1996, *ApJ*, 462, 576
- Eke, V. R., Navarro, J. F., & Steinmetz, M. 2001, *ApJ*, 554, 114
- Fall, S. M., & Efsthathiou, G. 1990, *MNRAS*, 193, 189
- Fimani, C., D'Onglia, E., Avila-Reese, V., Chincarini, G., Hernandez, X., Chincarini, G. 2000, *MNRAS*, 315, L29
- Gardner, J. P. 2001, *ApJ*, 557, 616
- Ghigna, S.; Moore, B., Govevato, F.; Lake, G., Quinn, T., & Stadel, J. 2000, *ApJ*, 544, 616
- Gnedin, O. Y., Hernquist, L., & Ostriker, J. 1999, *ApJ* 514, 109
- Gnedin, O. Y., & Ostriker, J. 1999, *ApJ*, 1999, 513, 626
- Rebel, E. K. 1999 *IAU Symp.* 192, 17-38, Cape Town, in press, eds. W. Hitecock, P. & Cannon (Gr99)
- Rebel, E. K., 2001, to appear in "Dwarf Galaxies and their Environment", Bad Honnef Workshop, January 2001, eds. K. S. de Boer, R. J. Dettmar, & U. Klein, Shaker Verlag, in press
- Haiman, Z., Rees, M., & Loeb, A. 1996, *ApJ*, 467, 522
- Haiman, Z., Thoul, A., & Loeb, A. 1996, *ApJ*, 464, 523
- Hargreaves, J. C., Gilmore, G., Irwin, M. J., Carter, D. 1994a, *MNRAS* 269, 957
- Hargreaves, J. C., Gilmore, G., Irwin, M. J., Carter, D. 1994b, *MNRAS* 271, 693
- Hargreaves, J. C., Gilmore, G., Annan, J. D. 1996a, *MNRAS* 279, 108
- Helmi, A., & White, S. D. M. 1998, *MNRAS*, 402, 53
- Helmi, A., White, S. D. M., de Zeeuw, P., & Zhao, H. 1999, *Nature*, 402, 53
- Hernquist, L. 1993, *ApJS*, 86, 289
- Ibata, R. A., & Lewis, G. F. 1998, *ApJ*, 500, 575
- Ibata, R. A., Lewis, G. F., Irwin, M., Totten, E., & Quinn, T. 2001, *ApJ*, 551, 295
- Ibata, R. A., Irwin, M., Lewis, G., Ferguson, A., Tanvir, N. 2001, *Nature*, 409, 49
- Irwin, M., & Hatzidimitriou, D. 1995, *MNRAS*, 277, 1354
- Johnston, K. V., Sigurdsson, S., & Hernquist, L. 1999, *MNRAS* 301, 771
- Johnston, K. V., Zhao, H., Spergel, D. N., & Hernquist, L. 1999, *ApJL*, 512, L109
- Johnston, K. V., Sackett, P. D., & Bullock, J. 2001, *ApJ*, 557, 137
- Klessen, R., & Kroupa, R. 1998, *ApJ*, 498, 143
- Klypin, A., Klypin, A. V., Valenzuela, O., & Prada, F. 1999, *ApJ*, 522, 8
- Kroupa, P., & Bastian, U. 1997, *New A* 2, 139
- Kuhn, J. R., & Miller, R. H., 1989, *ApJL*, 341, 41
- Kuhn, J. R., 1993, *ApJL*, 409, 13
- Lake, G., Skillman, E. D. 1989, *AJ* 98, 1274
- Lake, G., 1990, *MNRAS*, 244, 701
- Majewski, S. R., Olszewski, J. C., Patterson, R. J., Kunkel, W. E., Johnston, K. V., & Geisler, D. 2000, *AJ*, 119, 760
- Martinez-Delgado, D., Aparicio, A., Gomez-Flechoso, M. A., 2001, to appear on *ApJL*
- Mateo, M. 1998, *ARA A*, 36, 435
- Mayer, L., Govevato, F., Colpi, M., Moore, B., Quinn, T., Wadsley, J., Stadel, J., & Lake, G. 2001a, *ApJL*, 547, L123
- Mayer, L., Govevato, F., Colpi, M., Moore, B., Quinn, T., Wadsley, J., Stadel, J., & Lake, G. 2001b, to appear on *ApJ*, Oct 1st issue
- McGaugh, S., Rubin, V., & de Blok, E., 2001, astro-ph/0107326, to appear on *AJ*
- Mihos, C., Dubinski, J., & Hernquist, L. 1998, *ApJ*, 502, 141
- Mihos, J. H., Mao, S., & White, S. D. M. 1998, *MNRAS*, 296, 847
- Moore, B., & Davis, M. 1994, *MNRAS*, 270, 209
- Moore, B., Katz, N., & Lake, G. 1996, *ApJ*, 457, 455
- Moore, B., Ghigna, S., Govevato, F., Lake, G., Quinn, T., Stadel, J., & Tozzi, P. 1999, *ApJL*, 524, L19-L22
- Moore, B., Quinn, T., Govevato, F., Stadel, J., & Lake, G. 1999, *MNRAS*, 310, 1147
- Moore, B., Gelato, S., Jenkins, A., Pearce, F. R., Quilis, V. 2000, *ApJ*, 535, L21
- Moore, B. 2001, Plenary talk, 20th Texas Symposium, eds. J. C. Wheeler & H. Martel
- Moore, B., Calcanoe-Roldan, C., Stadel, J., Quinn, T., Lake, G., Ghigna, S., Govevato, F. 2001, *Phys. Rev. D*, in press
- Odenkirchen, M. et al. 2001, to appear on *ApJ*
- Peebles, J. E. 2000, *ApJ*, 534, L127
- Peebles, P. J. E., & Vilenkin, A. 1999, *Phys. Rev. D* 60, 103506
- Piatek, S., Pryor, C. 1995, *AJ*, 109, 1071
- Piatek, S., Pryor, C., Amato, T. E., Olszewski, E. W. 2001, *AJ*, 121, 841
- Pryor, C. 1994, see Meylan & Prugniel 1994, 323
- Schweitzer, A. E., Cudworth, K. M., Majewski, S. R., Suntzeff, N. B. 1995, *AJ* 110, 2747
- Schweitzer, A. E., Cudworth, K. M. 1996, in the American Astronomical Society Meeting, 188, 09.01
- Spergel, D. N., Steinhardt, P. J. 2000, *Phys. Rev. Lett.*, 84, 3760
- Springel, V., & White, S. D. M. 1999, *MNRAS*, 307, 162
- Tegmark, M., Silk, J., Rees, M., Blanchard, A., Abel, T., & Palla, F. 1997, *ApJ*, 474, 1
- Toomre, A., & Toomre, J. 1972, *ApJ*, 178, 623
- Van den Bosch, F. C., Robertson, B. E., Dalcanton, J., & de Blok, W. J. G. 2000, *AJ*, 119, 1579
- Warren, M. S., Quinn, P. J., Salmon, J. K., Zurek, W. H. 1992, *ApJ*, 399, 40
- White, S. D. M., & Frenk, C. S. 1991, *ApJ*, 379, 52
- Vivas, A. K., et al., 2001, *ApJ*, 554, L33
- Yoshida, N., Springel, V., White, S. D. M., & Toomre, B. 2000a, *ApJL*, 535, L103
- Yoshida, N., Springel, V., White, S. D. M., & Toomre, B. 2000a, *ApJL*, 544, L87
- Zhao, H., Johnston, K. V., Hernquist, L., & Spergel, D. N. 1999, *A & A*, 348, L49